J Mater Sci (2008) 43:5265–5273
DOI 10.1007/s10853-008-2773-0

Effects of the enhanced heat treatment on the mechanical properties and stress corrosion behavior of an Al–Zn–Mg alloy

Min Song · Kanghua Chen

Received: 12 January 2008 / Accepted: 2 June 2008 / Published online: 17 June 2008

Abstract In this article, the effects of the enhanced solution treatment (EST) and high-temperature pre-precipitation (HTPP) on the microstructures, mechanical properties, and stress corrosion cracking resistance of an Al–Zn–Mg alloy have been investigated. The results indicated that EST and HTPP can substantially affect the microstructures of the alloy. The width of the continuously distributed grain boundary precipitates decreases after the EST, while the continuous grain boundary precipitation changes to a discontinuous precipitation structure after both the EST and HTPP. The yield strength, tensile strength, elongation, and fracture toughness of the specimens after the EST are much higher than those of the specimens only after traditional solution treatment, since the EST substantially decreases the size and volume fraction of the constituents. The stress corrosion cracking resistance of the specimens after both the EST and HTPP has been greatly improved due to the discontinuous distribution, and high Cu and low Mg concentrations of the grain boundary precipitates.

Introduction

Al–Zn–Mg series alloys have been widely used as structural materials in aeronautical industries due to the attractive combined properties, such as low density, high yield stress, ductility, and fatigue resistance [1, 2]. However, these series alloys are sensitive to stress corrosion cracking (SCC) in sodium chloride solutions, which substantially restricts their further applications. The mechanism of SCC in the Al–Zn–Mg alloys is generally attributed to anodic dissolution of the grain boundary region exacerbated by the stress [3], accompanied by the hydrogen embrittlement [4]. The study of Song et al. [4] showed that the segregation of Mg and H decreases the grain boundary strength, hence resulting in grain boundary embrittlement, while H embrittles the grain boundary more seriously than Mg for the same segregation concentration.

It is known that the SCC resistance can be improved by T73 temper (overaging). However, as compared to T6 temper, the strength of the alloy is reduced by 10–15%. Previous investigations [2, 5, 6] showed that 7055/7075-T77 (retrogression and retrogression reaging) plates and extrusions offer not only increased strength, but also enhanced resistance to exfoliation corrosion, improved fracture toughness, and excellent resistance to the growth of fatigue cracks, compared to 7150-T6 alloy. The attractive combined properties of 7055/7075-T77 were not only attributed to the high ratios of the Zn/Mg and Cu/Mg, but also to the T77 temper, which provides a microstructure at and near grain boundaries that is resistant to both intergranular fracture and intergranular corrosion combined with a matrix microstructure that resists the localization of strain while also offering enhanced resistance to the passage of mobile dislocations [5, 6]. Huang et al. [7] showed that a high-temperature pre-precipitation (HTPP) treatment can enhance the distribution discontinuity of the grain boundary precipitates, increase the Cu concentration in the grain boundary precipitates, and lead to the enhanced resistance to the intergranular and exfoliation corrosion. The critical stress intensity factor in salt solutions has also been increased with the same strength and ductility. In a very recent paper, Ou et al. [8] developed a new heat treatment process using step-homogenization,

M. Song (✉) · K. Chen
State Key Laboratory of Powder Metallurgy, Central South University, Changsha 410083, China
e-mail: min.song.th05@alum.dartmouth.org

step-quenching, and aging treatment to obtain a microstructure exhibiting a T6 matrix precipitation and T73 grain boundary precipitates. Similar to T77, the process can improve the SCC resistance of the 7050 aluminum alloy without degrading the strength. However, the process cannot be used on 7075 aluminum alloy due to the inborn high quench sensitivity of 7075 alloy. Although proper temper (T77) can substantially improve the properties of the Al–Zn–Mg alloys, the processing of the alloys is difficult because of the high alloying element concentration. A considerable number of soluble constituents remain in the alloy after conventional processing due to the concentrations of the alloying elements over the limit of the solid solubility [5, 7, 9, 10]. The constituents in the matrix can improve crack initiation and propagation, thus decreasing the fracture toughness and SCC resistance of the Al–Zn–Mg alloys.

In this article, a series of the enhanced solution treatments (EST), accompanied by the HTPP, have been developed, and their influences on the mechanical properties and stress corrosion behavior of an Al–Zn–Mg alloy have been studied.

Experimental

The nominal composition of the alloy used in the present study has been shown in Table 1. The alloy was prepared in an induction furnace in an argon atmosphere. The as-cast ingot was homogenized at 455 °C for 10 h, followed by air cooling to room temperature. Then the ingot was converted into rods by hot extrusion at 450 °C, with an extrusion ratio of 9:1. The extruded rods were solution treated under a series of conditions, followed by cold water quenching (room temperature, 20 °C) and aging treatments (120 °C for 24 h). The solution treatments include the traditional solution treatment, the EST, and HTPP. Detailed description of the solution treatment can be found in Table 2. To avoid melting of some multi-phase eutectic located at grain boundaries, the EST uses an increasing temperature method from 450 to 480 °C instead of the isothermal treatment at 480 °C. The prior dissolution of the multi-phase eutectic during the EST enhances the melting point temperature, and thus allows a further high-temperature solution treatment to be used.

Table 1 Nominal composition of the tested Al–Zn–Mg alloy (mass fraction, %)

Zn	Mg	Cu	Mn	Zr	Al
4.5	3.3	0.15	0.25	0.2	Bal.

The mechanical properties were tested at room temperature using a smooth dog-bone-shaped tensile specimen that had a gage size of 6 mm in diameter and 40 mm in length conforming to GB/T 6397. All the specimens have an axis along the extrusion direction. The tensile ductility (δ, strain to fracture), yield strength ($\sigma_{0.2}$), and tensile strength (σ_b) were determined at a constant strain rate of 5×10^{-4} s^{-1} by an Instron-8032 testing machine. Strictly conforming to GB4161-84, plain strain fracture toughness (K_{IC}) tests were performed in three-point bending using rectangular cross-section specimens with dimension of 120 mm in length, 10 mm in height, and 7 mm in thickness. Specimens were fatigue cracked prior to fracture toughness experiments, at a constant ratio ($R = K_{min}/K_{max}$) of 0.1 and under decreasing stress intensity conditions.

The SCC resistance of the specimens after various solution treatments and aging treatment was performed using double cantilever beam (DCB) testing method. The DCB specimens were exposed to a sodium chloride solution (3.5% NaCl in distilled water) after being loaded with opposing bolts. Crack propagation was along the extruded direction. The length of the crack and the propagation time were measured on the specimen side using a traveling

Table 2 The procedures of the solution treatments

Solution type	Traditional solution treatment	Enhanced solution treatment (EST)	High-temperature pre-precipitation (HTPP)
S1	450 °C/2 h	–	–
S2	450 °C/2 h	Increasing temperature to 465 °C with a rate of 5 °C per hour	–
S3	450 °C/2 h	Increasing temperature to 480 °C with a rate of 5 °C per hour	–
S4	450 °C/2 h	Increasing temperature to 480 °C with a rate of 5 °C per hour	Decreasing temperature to 430 °C with a rate of 30 °C per hour
S5	450 °C/2 h	Increasing temperature to 480 °C with a rate of 5 °C per hour	Decreasing temperature to 400 °C with a rate of 30 °C per hour
S6	450 °C/2 h	Increasing temperature to 480 °C with a rate of 5 °C per hour	Decreasing temperature to 370 °C with a rate of 30 °C per hour

microscope. The stress intensity factor K_I was calculated according to the following equation:

$$K_I = \frac{Edh\left[3h(a+0.6h)^2 + h^3\right]^{1/2}}{4\left[(a+0.6h)^3 + h^2 a\right]} \quad (1)$$

where E is the elastic modulus, d the displacement, h the half height of the specimen, and a is the crack length.

The as-solution-treated and aging-treated microstructures were studied by optical microscopy (OM) and transmission electron microscopy (TEM), while the fracture surface after tensile testing was studied by scanning electron microscopy (SEM, JSM-5600 LV), along with energy dispersive spectroscopy (EDS), to determine the composition of the coarse particles. The TEM specimens were prepared by twin jet electro-polishing in a 30% nitric acid−70% methanol solution at −35 °C and examined in a JEM-100CXII microscopy operating at 100 kV.

Results

Microstructures after solution treatment

Figure 1 shows the optical microstructures of the tested alloy after various solution treatments. It can be seen that a large number of the constituents exist in the matrix (both along the grain boundaries and in the grain interiors) after traditional solution treatment (S1, Fig. 1a), while the number and the aggregation of the constituents have been substantially decreased after the EST (S2 and S3, Fig. 2b, c). In aluminum alloys, the constituents result from the presence of Fe and Si impurities or major alloying elements, and are normally 1–5 vol.% in volume fraction and 1–30 μm in size [11, 12]. It can be seen from Fig. 1 that the higher the ending temperature of the EST, the less the number of the constituents. These results indicate that the application of the EST facilitates the dissolution of the

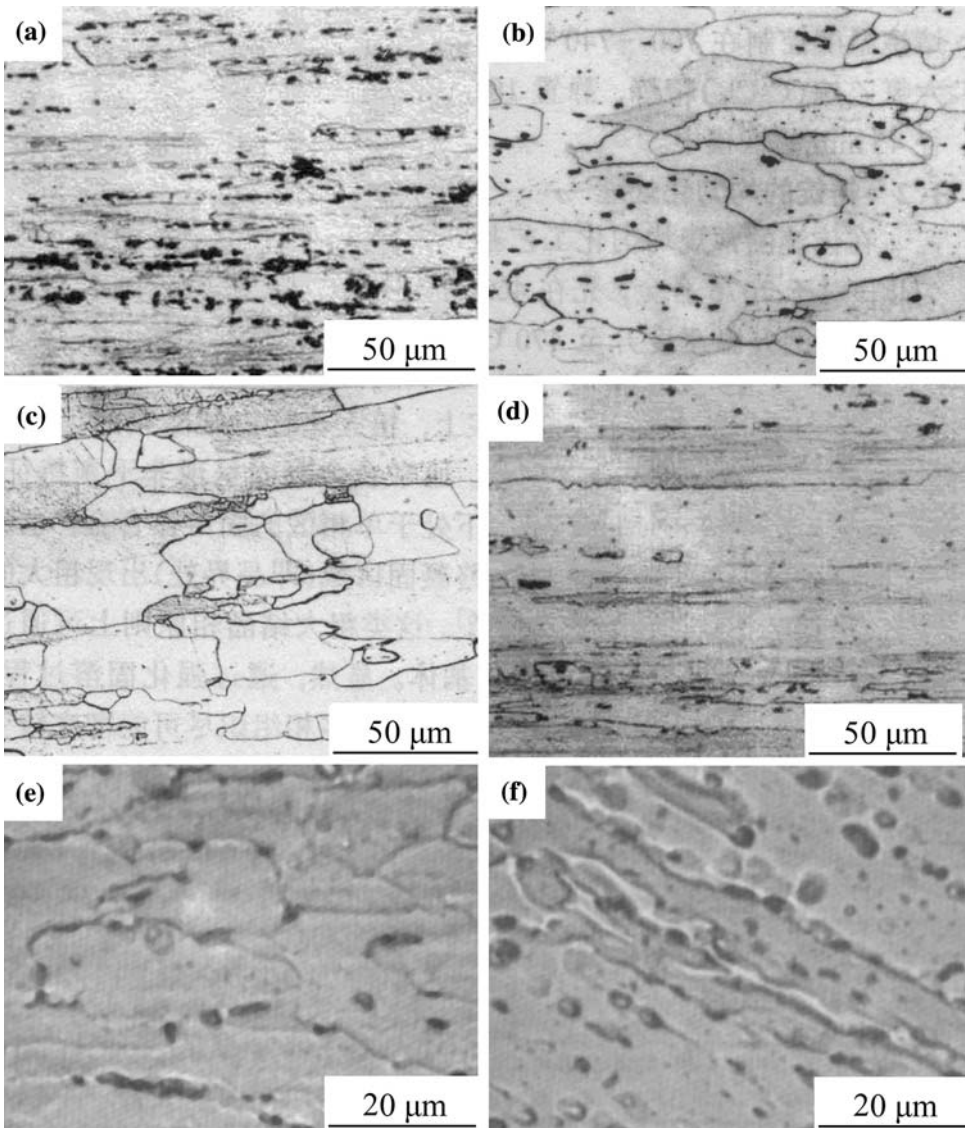

Fig. 1 OM images of the Al–Zn–Mg alloy after (**a**) S1, (**b**) S2, (**c**) S3, (**d**) S4, (**e**) S5, and (**f**) S6 treatments

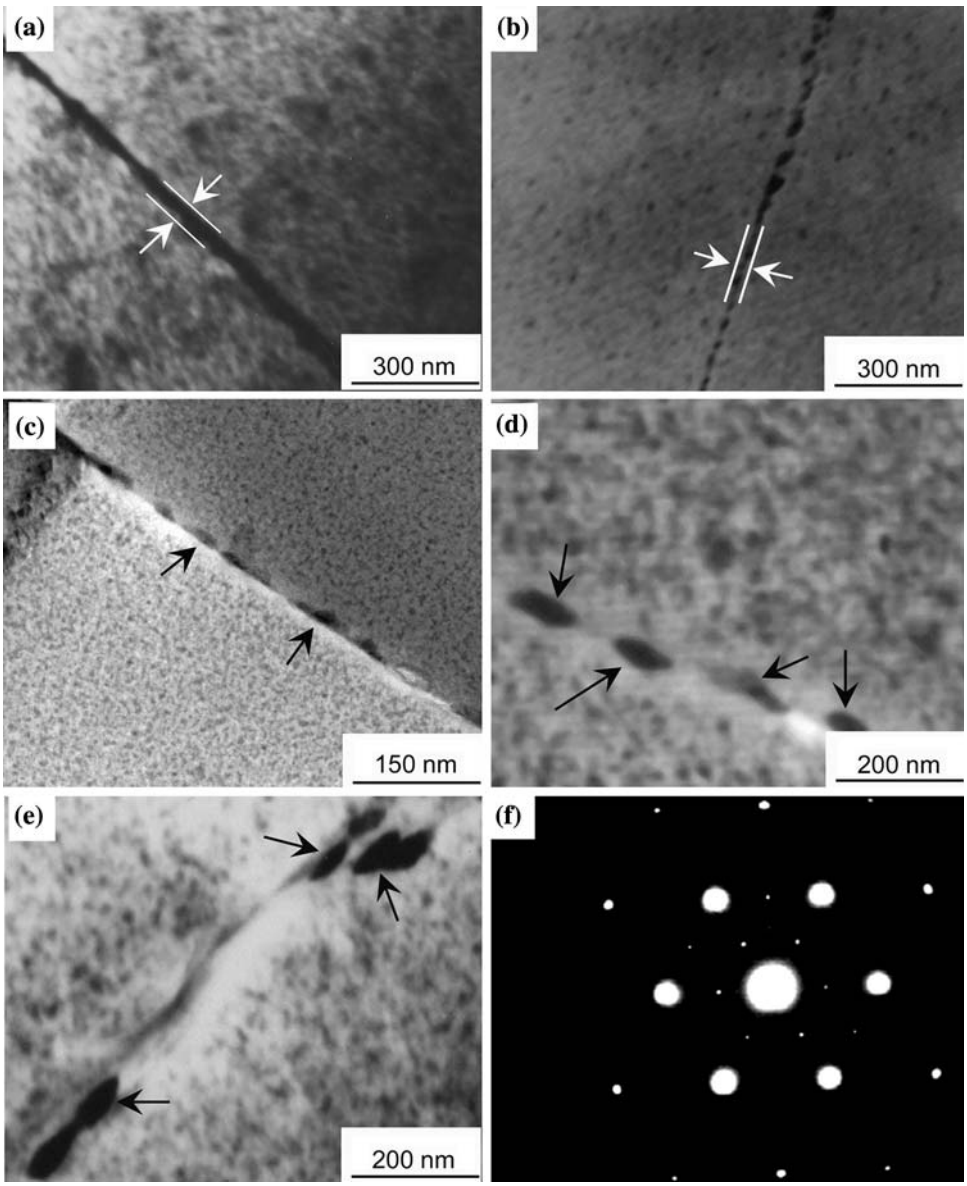

Fig. 2 TEM images of the Al–Zn–Mg alloy after (**a**) S1, (**b**) S3, (**c**) S4, (**d**) S5, (**e**) S6 and aging treatments and (**f**) the SADPs of the η' phase

soluble constituents and hence the decrease in the volume fraction of the constituents.

It can also be seen from Fig. 1 that the HTPP, accompanied by the EST, can increase the volume fraction of the large-sized particles in the alloy. The volume fraction of the particles after S3 treatment is very small, while it increases after various HTPP treatments (S4, S5, and S6, Fig. 1d–f). The distribution of the particles after the HTPP is generally along the grain boundaries, instead of the grain interiors. This exhibits a constitutive difference between the microstructures before and after the HTPP treatments. It is clearly seen that the constituents are distributed both along the grain boundaries and in the grain interiors after S1 or S2 treatments, while the large-sized particles are mainly distributed along the grain boundaries after S5 or S6 treatments. The lower the ending temperature of the HTPP, the larger the size and volume fraction of the particles along the grain boundaries.

Microstructures after aging treatment

Figure 2 shows the TEM microstructures of the alloy after solution and aging treatments. It is clearly seen that the EST and HTPP have important effects on the microstructures of the Al–Zn–Mg alloy. Although the structure in the grain interior remains similar (semi-coherent η' precipitates distribute uniformly in the grain interiors), major differences exist along the grain boundaries after various heat treatments. For the specimen after traditional solution treatment (S1, without the EST and HTPP) and aging, the stable η precipitates distribute continuously along the grain boundaries (Fig. 2a). However, the EST can substantially

Table 3 Mechanical properties of the alloy after various solution treatments and aging treatment

Treatment	σ_b (MPa)	$\sigma_{0.2}$ (MPa)	δ (%)	K_{IC} (MPa $m^{1/2}$)
S1 + aging	551	472	13.5	26.4
S2 + aging	589	505	14.7	29.7
S3 + aging	613	536	15.5	35.5
S4 + aging	575	498	13.2	28.4
S5 + aging	559	489	12.7	27.1
S6 + aging	492	430	8.6	21.3

Note: All the data are the average values from three tests

decrease the width of the grain boundary precipitation belt (Fig. 2b). Most importantly, a discontinuous grain boundary precipitate structure can be achieved after both the EST and HTPP (Fig. 2c–e). The degree of the discontinuous distribution becomes more severe with the decrease in the ending temperature of the HTPP. At the same time, the size of the discontinuous precipitates also becomes larger, accompanied by a wider particle-free zone along the grain boundaries. Figure 2f shows the SADPs of the main strengthening phase (η' precipitates).

Mechanical properties

Table 3 illustrates the mechanical properties of the specimens after various heat treatments. It can be seen that the EST substantially improves the yield strength, tensile strength, tensile ductility, and fracture toughness. It can also be seen that the combined effects of the EST and HTPP on the mechanical properties of the specimens strongly depend on the ending temperature of the HTPP. The yield strength and tensile strength are slightly higher for the specimens after S4 and S5 treatments, while the elongation and the fracture toughness remain almost the same compared to the specimen after S1 treatment. However, the yield strength, tensile strength, elongation, and fracture toughness are much lower for the specimens after S6 treatment, compared to the specimen after S1 treatment, which indicates that the mechanical properties will be severely decreased if the ending temperature of the HTPP is too low. All the data indicate that the EST has beneficial effects on the mechanical properties of the alloy, while the HTPP degrades the mechanical properties of the alloy in someway.

Fracture surfaces

Figure 3 illustrates the fracture surfaces of the alloy after tensile testing to fracture. It can be seen that the fracture surface contains variously sized dimples and intergranular cracks for all the conditions. In addition, the coarse dimples contain secondary constituents, with some of the large constituents being fractured. It is evident from Fig. 3 that the coarse constituents fracture first and act as the microcrack sources. Previous studies [5, 13] also verified this kind of mixed fracture, in which fracture is initiated at large-sized second phase particles (constituents) and links up along the matrix grain boundaries. Thus, compared to the specimens after traditional solution treatment (S1), the improved tensile ductility and fracture toughness of the specimens after the EST (S2 and S3) are due to the small volume fraction and size of the constituents. However, the tensile ductility and fracture toughness are decreased for the specimens after the combined EST and HTPP, compared to the specimens only after the EST due to the large-sized precipitates along the grain boundaries, which also nucleate microcracks during deformation.

Stress corrosion behavior

The dependence of the crack propagation rate (v) on the stress intensity factor (K_I) of the tested alloy under various heat-treatment procedures is shown in Fig. 4. It can be seen that the crack propagation rate of the specimen after S3 treatment is lower than that of the specimen after S1 treatment at all testing stages, which indicated that the EST can evidently improve the stress corrosion resistance of the Al–Zn–Mg alloy due to the narrow width of the grain boundary precipitation belt. It can also be seen that accompanied by the EST, the HTPP can further improve the stress corrosion resistance of the alloy, since the crack propagation rate for the specimen after S5 or S6 treatment is much lower than that for the specimen after S3 treatment. The K_{ISCC} value ($\sim$8.7 MPa $m^{1/2}$) of the specimen after S3 and aging treatments is much lower than the K_{ISCC} values ($\sim$10.5 MPa $m^{1/2}$) of the specimens after S5/S6 and aging treatments.

Discussion

Effect of the microstructures on the mechanical properties

Precipitation strengthening is the primary mechanism in the Al–Zn–Mg alloys. The main aging sequence at temperatures below 463 K is usually given as: supersaturated solid solution → G.P. Zones → η' ($MgZn_2$) → η ($MgZn_2$) [14–17], and the main strengthening precipitates are the G.P. zones and the η' phase. In general, two aging peaks will be observed for the Al–Zn–Mg alloys during aging treatment (sometimes only one peak will be observed due to the overlapping) [4]. The first aging peak is associated with a high density of the coherent G.P. zones in the

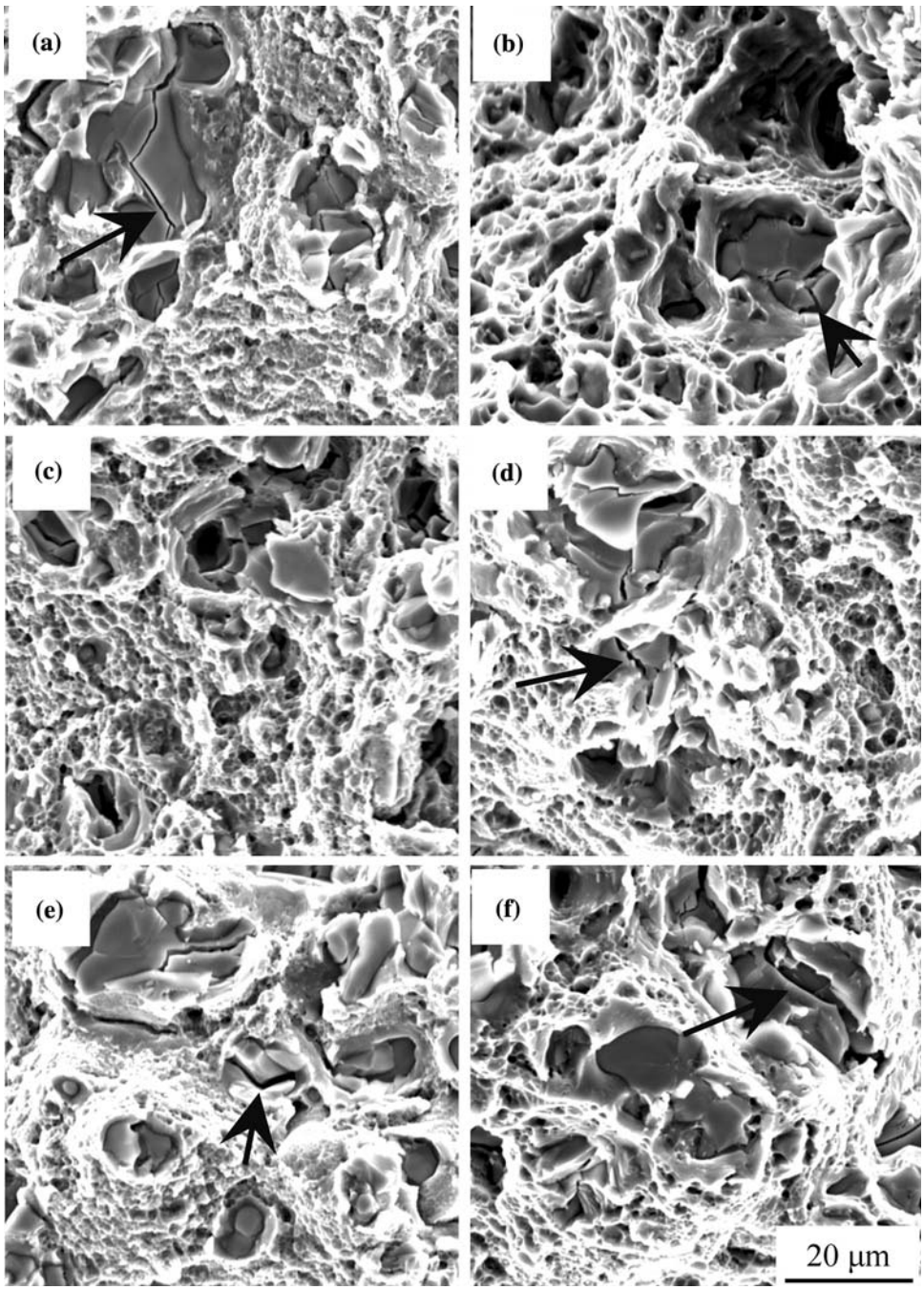

Fig. 3 SEM tensile surfaces of the alloy after (**a**) S1, (**b**) S2, (**c**) S3, (**d**) S4, (**e**) S5 and (**f**) S6 treatments and aging treatment

matrix. Since the G.P. zones are soft and weak, the strength of the first peak aged stage is significant only when the G.P. zone density is high. The increase in strength is due to the increase in surface energy when a dislocation cuts the G.P. zone. On further aging, the strength decreases caused by the dissolving of the G.P. zones. The second peak is associated with the η' phase. Since the η' phase is semi-coherent, the dislocations can only bypass the η' phase (Orowan mechanism). The peak value of the second peak aged stage equals or is larger than that of the first peak aged stage because the work done by an external force when dislocations bypass the η' phase is larger than that when the dislocations cut the G.P. zones. The peak value of the second peak is determined by the interspacing and the volume fraction of the η' precipitates according to the Orowan mechanism. Smaller interspacing and larger volume fraction of the precipitates are associated with the higher strength.

As observed from Figs. 1 and 2, the EST substantially decreases the volume fraction and size of the soluble constituents. Previous studies [11, 12] indicated that the coarse constituents are brittle and have low fracture

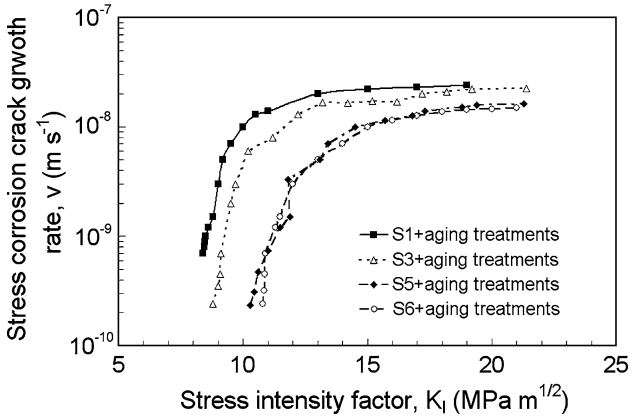

Fig. 4 Crack propagation rate versus crack tip stress intensity in 3.5% NaCl solution for the tested alloy

Table 4 Composition of the cracking constituents (wt.%)

Al	Fe	Si	Cu	Mn
62.2	10.1	11.5	5.9	10.3

strength and, thus, generate microcracks during deformation (also see arrows in Fig. 3). The larger the volume fraction of the constituents, the lower the tensile ductility and fracture toughness. The constituents normally result from the presence of the Fe and Si impurities or excess amounts of major alloying elements such as Mg, Zn, and Cu [11, 12]. Table 4 lists the chemical composition of the cracking constituents on the fracture surfaces in Fig. 3 using EDS analysis results. It can be seen that these cracking formation phases contain Fe, Si, and Cu. Thus, the EST can substantially improve the mechanical properties of the alloy by two mechanisms. First, the tensile ductility and fracture toughness have been improved since the EST decreases the number of the microcrack sources (volume fraction of the constituents). Second, the volume fraction of the strengthening precipitates has been increased after the EST. From Table 2, we know that the EST has a higher solution temperature than the traditional solution treatment. When the specimens are solution treated at a high temperature, more alloying atoms (including the alloying elements from the soluble constituents) dissolve into the matrix as solute atoms. Through water quenching, these atoms remain in a supersaturated state in the matrix. Thus, the driving force is also higher during the subsequent aging process, and a higher volume-fraction of precipitates and a lower volume-fraction of constituents will be obtained for the material.

It can also be seen from Figs. 1 and 2 that the HTPP substantially increases the large-sized precipitates along the grain boundaries. These large-sized grain boundary precipitates also nucleate microcracks during deformation (see Fig. 3). Thus, the tensile ductility and fracture toughness of the specimens after both the EST and HTPP are lower than those of the specimens only after the EST, as illustrated in Table 3. In principle, the precipitation of large-sized phase along the grain boundaries decreases the concentrations of the alloying elements in the matrix and, thus, decreases the strength of the alloy.

Effect of the microstructures on the SCC resistance

In the Al–Zn–Mg alloys, the increase in yield strength is accompanied by the decrease in the SCC resistance during aging due to the difference in the precipitation along the grain boundaries and in the grain interiors. Generally, the precipitates at the peak-aged stage are η' phases, while there are η phases along the grain boundaries, which cause the potential difference between the grain boundaries and matrix. The mechanism of SCC in the Al–Zn–Mg alloy was generally attributed to anodic dissolution of the grain boundary region exacerbated by the stress [3], accompanied by the hydrogen embrittlement [4]. Once the microcracks are formed, they propagate along the grain boundaries very quickly due to the continuous distribution of the η phase along the grain boundaries. Thus, the SCC resistance can be improved through two methods. The first method is to decrease the potential difference between grain boundary and matrix, and the second method is to decrease the continuity of the grain boundary precipitates.

In the Al–Zn–Mg series alloys, there is a strong trend for heterogeneous precipitation along the grain boundaries due to the high energy of the grain boundaries. Thus, a continuous distribution of the stable precipitates (η phases) along the grain boundaries during aging process is the fundamental characteristic of the Al–Zn–Mg alloys. However, it can be seen from Fig. 2 that the continuous distribution of the grain boundary precipitates changes to a discontinuous distribution after the EST and HTPP. The precipitation of the Al–Zn–Mg alloy in the grain interiors and along the grain boundaries is controlled by the driving force. During HTPP, the temperature is much higher than the traditional aging temperature, thus the driving force in the grain interiors is not high enough for the nucleation of the precipitates. However, the driving force is high enough for the precipitation along the grain boundaries due to the high energy of the grain boundaries, which causes the nucleation of the coarse, discontinuously distributed precipitates (close to over-aged boundary structure). These coarse precipitates are accompanied by the PFZ along or near the grain boundaries since the solute atoms are exhausted during the HTPP. This discontinuous structure of the grain boundary improves the SCC resistance, since the microcracks propagation is inhibited due to the discontinuous structure and a larger size and spacing of the

grain boundary precipitates decrease the dissolution rate [18, 19]. This phenomenon has also been observed in previous studies [14, 20], in which the SCC resistance could be improved by increasing the size and spacing of the grain boundary precipitates and by widening the PFZ. Previous studies [21–23] also showed that a T77 (retrogression and retrogression reaging) temper can also form a discontinuous distribution of the grain boundary precipitates and, thus, improve the SCC resistance without much expense of the yield strength. The EST and HTPP, similar to the T77 temper, result in a microstructure in which the grain boundary exhibits an overaged condition, while the grain interior exhibits a peak-aged stage. This type of microstructure improves the SCC resistance without much expense of the yield strength and tensile strength. However, the EST and HTPP have advantages over T77 since they can be used in the industries, while T77 temper is difficult to be used due to the short period retrogression requirement [2, 19].

In principle, HTPP also changes the chemical composition of the grain boundary precipitates. Table 5 lists the composition of the grain boundary precipitates after various heat treatments. It can be seen that the composition of the precipitates along the grain boundaries remains similar for the specimens after the traditional treatment and the EST. However, HTPP substantially increases the Cu concentration and decreases the Mg concentration of the grain boundary precipitates. Using embedded atom method (EAM), Song et al. [4] determined that the increase of the Mg concentration along the grain boundaries decreases the SCC resistance of an Al–Zn–Mg alloy. Two possible mechanisms are associated with the effects of the Mg [4]. First, the Mg segregation at grain boundary reduces the strength of the grain boundary and accelerates the stress corrosion crack initiation and propagation, thus raising the SCC susceptibility of Al–Zn–Mg alloys. Second, Mg segregation enhances the hydrogen absorption and increases hydrogen at the grain boundary as a result of the Mg–H interaction, resulting in hydrogen embrittlement and leading to further grain boundary embrittlement. For Al–Zn–Mg alloys, the η phase is very active and anodic with respect to the film-covered matrix [24]. Previous studies [25, 26] showed that the addition of copper both dissolves in the matrix and enters the η phase along the grain boundaries, making both more noble. As a result the mixed potential at the crack tip shifts to a more noble value. Thus, based on the results of the previous studies [25, 26], the improvement of the SCC resistance of the specimens after both the EST and HTPP could also be attributed to the reduced rate of dissolution of the more noble precipitates (with high copper content) along the grain boundaries, or reduced rate of hydrogen ion reduction and hydrogen absorption at the crack tip at the more noble potential.

Table 5 Composition of the grain boundary precipitates after various heat treatments

Treatment	Al (at.%)	Mg (at.%)	Zn (at.%)	Cu (at.%)
S1 + aging	93.7	4.8	1.1	0.4
S2 + aging	93.8	4.7	1.1	0.4
S3 + aging	93.6	4.7	1.2	0.5
S4 + aging	12.8	2.8	57.6	26.8
S5 + aging	13.1	2.6	54.5	29.8
S6 + aging	15.5	2.7	53.6	28.2

Conclusion

This article studied the effects of the EST and HTPP on the microstructures, mechanical properties, and SCC resistance of an Al–Zn–Mg alloy. The following conclusions can be drawn:

1. The EST and HTPP substantially affect the microstructures of the alloy. The width of the continuously distributed grain boundary precipitates decreases after the EST, while the continuous grain boundary precipitation changes to a discontinuous precipitation structure after both the EST and HTPP.
2. The EST improves the yield strength, tensile strength, elongation, and fracture toughness of the specimens by decreasing the size and volume fraction of the constituents.
3. The HTPP, accompanied by the EST, substantially improves the SCC resistance of the alloy by enhancing the discontinuous distribution, and high copper and low magnesium concentrations of the grain boundary precipitates. The discontinuous distribution of the grain boundary precipitates inhibits the crack propagation by decreasing the dissolution rate.

Acknowledgements This work was supported by the Creative Research Group of National Natural Science Foundation of China (grant no. 50721003) and Hunan Provincial Natural Science Foundation of China (grant no. 07JJ3117).

References

1. Heinz A, Haszler A, Keidel C, Moldenhauer S, Benedictus R, Miller WS (2000) Mater Sci Eng A 280:102. doi:10.1016/S0921-5093(99)00674-7
2. Lukasak DA, Hart RM (1991) Aerosp Eng 11:21
3. Dix EH (1940) Trans AIME 137:11
4. Song RG, Dietzel W, Zhang BJ, Liu WJ, Tseng MK, Atrens A (2004) Acta Mater 52:4727. doi:10.1016/j.actamat.2004.06.023
5. Srivatsan TS, Anand S, Sriram S, Vasudevan VK (2000) Mater Sci Eng A 281:292. doi:10.1016/S0921-5093(99)00716-9

6. Cina BM (1974) US Patent 3,856,584
7. Huang LP, Chen KH, Li S, Song M (2007) Scr Mater 56:305. doi:10.1016/j.scriptamat.2006.09.028
8. Ou BL, Yang JG, Wei MY (2007) Metall Mater Trans A 381:760
9. Srivatsan TS, Vasudevan VK (1999) J Met 51:42. doi:10.1007/s11837-999-0011-0
10. Srivatsan TS, Sriram S, Veeraraghavan D, Vasudevan VK (1997) J Mater Sci 32:2883. doi:10.1023/A:1018676501368
11. Hahn GT, Rosenfield AR (1975) Metall Trans A 6:653. doi:10.1007/BF02672285
12. Thompson DS (1975) Metall Trans A 6:671. doi:10.1007/BF02672287
13. Ludtka GM, Laughlin DE (1982) Metall Trans A 13:411
14. Adler PN, Deiasi R, Geschwind G (1972) Metall Trans 3:3191. doi:10.1007/BF02661333
15. Lyman CE, Vander Sande JB (1976) Metall Trans A 7:1211. doi:10.1007/BF02656605
16. Marcantonio JA, Mondolfo LF (1970) J Inst Met 98:23
17. Mondolfo LF (1971) Met Mater 5:95
18. Kent KG (1969) J Inst Met 93:127
19. Wu YL, Froes FH, Alvarez A, Li CG, Liu J (1997) Mater Des 18:211. doi:10.1016/S0261-3069(97)00084-8
20. Poulose PK, Morral JE, McEvily AJ (1974) Metall Trans 5:1393. doi:10.1007/BF02646625
21. Park JK, Ardell AJ (1984) Metall Trans A 15:1531. doi:10.1007/BF02657792
22. Rajan K, Wallace W, Beddoes JC (1982) J Mater Sci 17:2817. doi:10.1007/BF00644656
23. Wang H, Cui H, Hao B, Cheng J, Huang J, Zhang J (2005) Acta Metall Sin 41:1267
24. Dix EH, Brown RH, Binger WW (1961) In: Lyman T (ed) Metals handbook, 8th edn., vol 1. ASM, Metal Park, OH, p 916
25. Busby J, Cleave JF, Cudd RL (1971) J Inst Met 99:41
26. Sarkar B, Marek M, Starke EA Jr (1981) Metall Trans A 12:1939. doi:10.1007/BF02643806